On-Demand Non-Contact Distillation: Low-g Demonstrations of a Leidenfrost Waste-Water Processor

Rawand M. Rasheed¹ and Mark M. Weislogel² *Portland State University, Portland, OR, 97201*

Leidenfrost phenomenon is employed as a potential solution to NASA's urine-water recovery problem by providing a method for on-demand non-contact distillation. Leidenfrost investigations have been almost exclusively conducted in terrestrial environments and are in turn largely defined by the ever-presence of gravity. In this work we demonstrate a variety of Leidenfrost effects for enormous liquid droplets in the microgravity environment of a 2.1 second drop tower. Dynamic Leidenfrost droplet impacts on a selection of heated hydrophilic and superhydrophobic surfaces in microgravity are presented. Nearly ideal elastic noncontact impacts and droplet oscillation modes are observed. Impact experiments are extended to a variety of heated substrates including macro-pillar arrays, confined passageways, and others. The potential for contamination-free processing is obvious, with the proof of concept to be pursued shortly.

Nomenclature

\boldsymbol{A}	= Area	\boldsymbol{x}	= Position	
c_p	= Specific heat	$\dot{\mathcal{X}}$	= Velocity	
g	= Gravitational acceleration	$\ddot{\mathcal{X}}$	= Acceleration	
h_{fg}	= Latent heat of vaporization			
ID	= Inner diameter	Greek l	Greek Symbols	
k	= Thermal conductivity	α	= Wedge half angle	
m	= Mass	δ	= Vapor layer thickness	
ṁ	= Mass flowrate	μ	= Dynamic viscosity	
\dot{m}_{evap}	= Evaporating vapor mass flowrate	ho	= Density	
OD	= Outer diameter	heta	= Angle	
Pr	= Prandtl number			
q	= Heat transfer	Subscri	Subscripts	
q_c	= Conduction heat transfer	а	= Air	
q_{fc}	= Forced convection heat transfer	d	= Droplet	
R	= Radius	f	= Final	
r	= Radius as a function of time	i	= Incident	
r_t	= First time derivative of radius	l	= Liquid	
t	= Time	0	= Initial	
T	= Temperature	R	= Reflection	
u	= Velocity	S	= Surface	
u_{vap}	= Evaporating vapor velocity	ν	= Vapor	
We	= Weber Number	∞	= Ambient Environment	

I. Introduction

The National Aeronautics and Space Administration has identified the separation and recovery of water from waste streams as a major challenge. NASA's technology roadmap has identified water recovery and management (TA 6.1.2) as an area in need of innovative technological solutions to enable human exploration into deep space. At least 98% water recovery from waste-water streams is required for such missions, a performance goal that is not yet attainable with current state of the art technology. It is also desirable to develop a water recovery system that significantly reduces the number of moving components, eliminates the need for urine storage, eliminates the need for addition of pretreat chemicals to urine, and unifies urine-brine processing. Herein, the foundations of a novel, non-contact, heat-driven distillation method are investigated as a potential method to address NASA's water recovery challenge.

¹Graduate Student/NSTRF Fellow, Mechanical and Materials Engineering, 1930 SW 4th Avenue

²Professor, Mechanical and Materials Engineering, 1930 SW 4th Avenue

Heat driven distillation is routinely employed to distill liquid-liquid and liquid-solute solutions. Such processes typically employ pool boiling. Film boiling is a less efficient boiling regime that is not usually exploited for distillation

purposes. In the pool boiling regime, liquid droplets deposited on substrates slightly above the liquid's boiling temperature will undergo nucleate boiling and will boil away in seconds. However, if the substrate temperature is significantly higher than the liquid's boiling temperature, the droplet will not undergo nucleate boiling, but will instead levitate on its own vapor layer. This vapor layer insulates the droplet from the heated substrate, reducing heat transfer to the liquid droplet by orders of magnitude. The levitating droplets are not in contact with the surface, eliminating nucleation sites for bubble formation. These combined effects increase droplet lifetimes by orders of magnitude. For example, a static

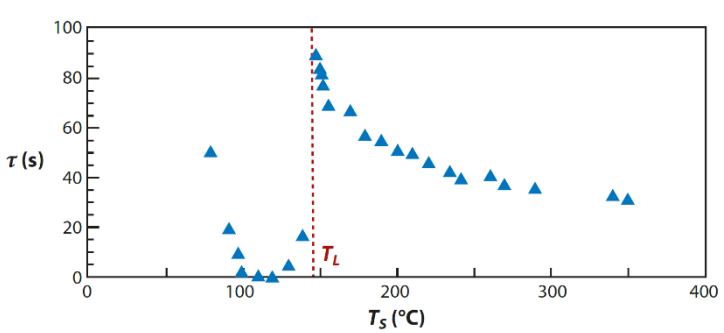


Figure 1: Lifetime plot for a 2 mm droplet of water deposited on a polished aluminum surface as a function of surface temperature, T_s . Figure from Quéré.²

0.03 mL water droplet on a planar aluminum substrate above 193°C will require several minutes to completely evaporate. This phenomenon is called the Leidenfrost effect. Figure 1 shows a droplet lifetime plot for a 2 mm diameter droplet of water on a polished aluminum surface at varying surface temperatures. The maximum droplet lifetime shown by the vertical line just below 150°C identifies the Leidenfrost point, the point of minimum heat flux.

Though exploiting Leidenfrost phenomena may seem a poor choice due to low evaporation heat transfer rate, employing this phenomenon to distill streams of droplets is of interest for spacecraft applications due to the noncontact nature of the phenomenon, potentially enabling fouling-free distillation. Further, heat driven Leidenfrost distillation potentially allows for streams of waste-water solutions to be distilled fully to dry salt. Distillation rates are also comparable to certain liquid production rates (i.e., astronaut urine production) permitting essentially real-time distillation of streams of droplets at elevated temperatures. Stamey and Mihara³ present experimental results for bacterial growth in sterile urine from human subjects. Results show that exponential bacterial growth occurs after two hours for all types of bacteria. Liquid solutions of urine processed essentially on-demand at temperatures in excess of 70°C ensure minimal microbial growth, reducing, if not eliminating the need for urine pretreat chemicals, which are used to significantly hinder the rate of bacterial growth in urine.

Leidenfrost droplets are highly mobile due to the vapor layer separating droplets from heated substrates. Viscous drag from the vapor layer is negligibly small leading to nearly frictionless motion across heated surfaces. Such mobility of Leidenfrost droplets encourages the possibility for competitive microgravity distillation system designs that employ heated conduits and a simple motive force for droplet streams in the form of airflow, pressure gradient, or the vapor production of the evaporating droplets themselves.

The Leidenfrost effect has been studied extensively for its relevance to numerous applications including spray cooling, fuel combustion, nuclear reactor cooling, jet and rocket engine propulsion, manufacturing of metals, and others. Figure 2-12 Biance et al. Investigated Leidenfrost phenomenon providing a scale expression for static Leidenfrost droplet lifetimes. The dynamics of Leidenfrost droplet impacts have been investigated in depth. It has been shown that the dynamic Leidenfrost point is a function of Weber number 16 as is the maximum spreading of the drops on impact. The Extensive experimental investigations quantifying heat transfer for dynamic Leidenfrost droplet impacts have been conducted 18-22 as well as mathematical considerations for heat transfer in the dynamic Leidenfrost mode. Leidenfrost droplet heat transfer and evaporation rates have also been experimentally investigated in the static case.

Maquet et al.²⁵ demonstrate that although the Leidenfrost point itself has a weak dependence on gravity level, Leidenfrost droplet lifetimes have a strong inverse dependence on gravity. Veldhoven and Capelleveen²⁶ show decreases in Leidenfrost temperature with decreasing ambient pressure. Chen et al.²⁷ show dramatic increases in dynamic Leidenfrost point temperature with increased levels of alcohol surfactants, showing that increases in the Leidenfrost point are due to decreasing surface tension.

Takata et al.²⁸ show increases in the Leidenfrost point with increased surface wettability. Kim et al.²⁹ report an increase and decrease in the Leidenfrost point for water on hydrophilic and hydrophobic surfaces, respectively. Kim et al.^{30,31} report significant increases in the Leidenfrost point of water as a result of impacts on porous and micropillared surfaces. Such surface structures are found to disrupt and collapse vapor layer formation. Similar observations have been documented for wetting microstructured surfaces³²⁻³⁵ as well as for surfaces consisting of carbon nanofibers.³⁶ Kwon et al.³⁷ report significant increases in the Leidenfrost point with decreasing micropillar density on

wetting surfaces. Significant reduction in Leidenfrost point has also been reported on microstructured non-wetting surfaces.^{38,39} Vakarelski et al.³⁹ report significant decreases in the Leidenfrost point on microstructured superhydrophobic surfaces due to vapor layer stabilization on such surfaces. Kim et al.²⁹ also develop mathematical predictions for the dynamic Leidenfrost point on structured surfaces.

Exploratory low-gravity Leidenfrost behavior has been pursued in drop tower tests. 40,41 Rasheed and Weislogel 48 present facile production methods for superhydrophobic surfaces, including thermally stable surfaces, which are utilized in this study. Superhydrophobic surfaces were also shown to reduce fouling of surfaces resulting from streams of urine by a factor of 30. In this work, Leidenfrost droplet modes of transport under varying conditions in microgravity are presented. Microgravity drop tower experiments include dynamic Leidenfrost impacts of oscillation free droplets on surfaces with varied wettability under varying impact conditions, droplet transport modes through conduit bends, and millimetric Leidenfrost vapor layer formation in a unique low-g Leidenfrost regime. Mathematical models are presented that predict Leidenfrost vapor recoil force and vapor layer thickness in the absence of gravity. Results for experimental investigations extending terrestrial Leidenfrost droplet lifetime experiments for dynamically rolling droplets on heated substrates are also presented. The self-cleaning nature of fouled, superheated, superhydrophobic surfaces is also observed and reported herein. A model that predicts Leidenfrost droplet lifetime for droplets in the dynamic rolling mode in a terrestrial gravity environment is developed, showing good prediction of experimental results. These results have practical design implications for potential spacecraft applications.

II. Experimental

A. Drop Tower and Function

A drop tower⁴² is employed in this work to simulate microgravity conditions. An image of the drop tower is shown



Wollman and Weislogel.⁴³

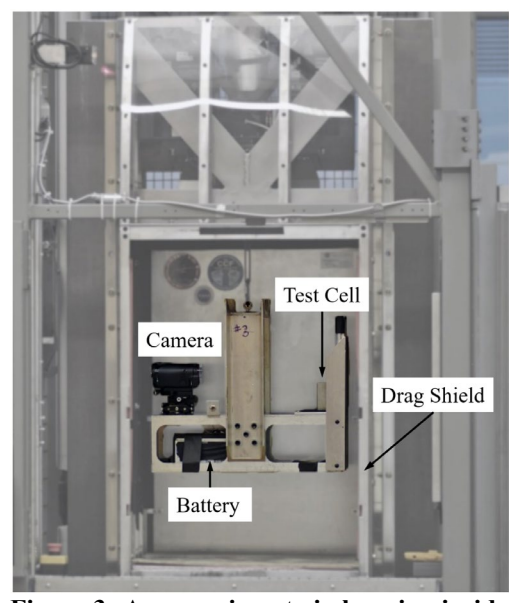


Figure 3: An experiment rig hanging inside the drag shield of the drop tower. Both the experiment rig and the drag shield are Figure 2: The 2.1 s Dryden Drop released at the same time. The experiment Tower (DDT). Image from rig is allowed to fall freely inside the drag shield. Image from Torres.46

in Fig. 2. A touch screen computer allows a single operator to safely operate the drop tower assisted primarily by automated functions for quick experiment turn around with up to ~ 20 drops per hour. An experiment rig is installed into a drag shield and released into freefall for 2.1 s. Figure 3 shows an example of an experiment rig inside the drag shield. The experiment rig and drag shield are released simultaneously. The drag shield is guided by two noncontacting cables. Two metal fins mounted to the sides of the drag shield pass through permanent magnets at the base of the tower. The relative motion between parallel magnetic fields and drag shield fins generate eddy currents in the fins that resist the motion and decelerate the falling masses which come to on foam pads. Wollman⁴⁴ for further details.

B. Microgravity Droplet Generators

A microgravity, oscillation-free, droplet generator, referred to as a 'Logan Shooter,' is employed in the dynamic Leidenfrost impact experiments in microgravity. The Logan shooter consists of two superhydrophobic surfaces forming a wedge. The inside surfaces of the wedge are coated with a commercially available, one-step superhydrophobic Cytonix WX2100 spray, which is a fluorine-based Teflon coating. Contact angles greater than 150° are produced on the inside surfaces. A volume of water is dispensed near the narrowest point of the wedge. Large liquid volumes form puddles. At initiation of the drop tower test, the 'puddle' jumps from the surface in an attempt to establish a sphere. However, the water is confined by the wedge which induces a capillary pressure gradient in the droplet that forces it out of the wedge. Oscillations in the drop are substantially damped during the ejection process. Figure 4 shows (a) a schematic of the Logan shooter and (b) a Logan Shooter with a 5° half angle ejecting a 10 mL droplet of water. Torres⁴⁵ provides further details.

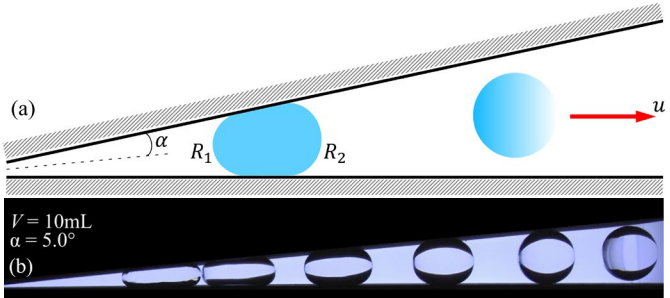


Figure 4: (a) Schematic of a Logan Shooter. A droplet confined between two superhydrophobic plates. (b) Drop tower demonstration of a Logan Shooter with 5° half-angle ejecting a non-oscillating 10 mL water droplet. Image from Torres.⁴⁵



Figure 5: Spontaneous capillary rise and ejection of 5 cS PDMS in a circular tube with nozzle. Figure from Wollman.⁴⁴

The Logan Shooter requires superhydrophobic non-wetting surfaces to function properly. For purposes of conducting dynamic Leidenfrost droplet impact experiments with wetting liquids such as ethanol, the method of passive capillary droplet ejection through a converging circular tube is employed as studied by Wollman. ⁴⁴ Fluids with contact angle θ less than 90° rise to considerable heights in tubes in microgravity. Adding a nozzle to the end of the

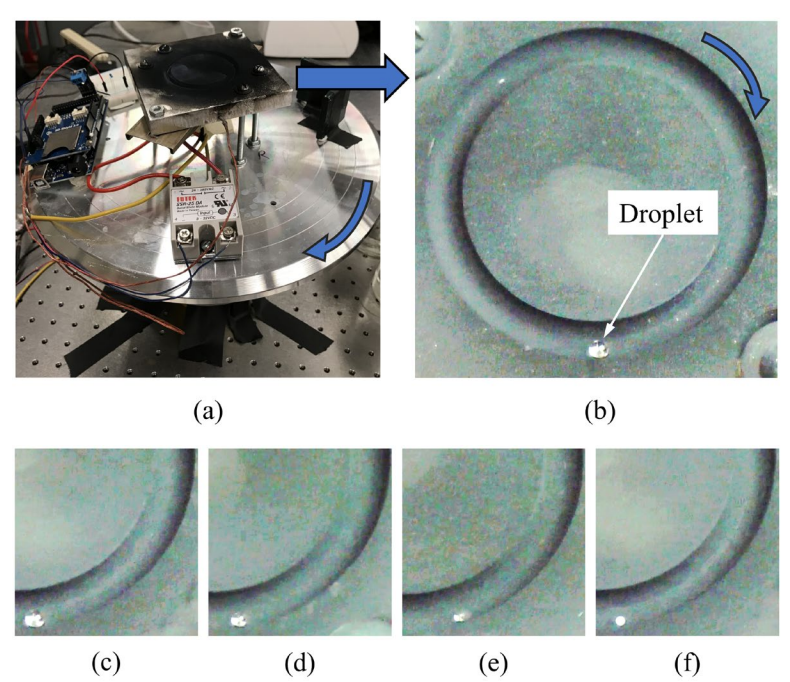


Figure 6: (a) Image of the experimental setup with the blue arrow pointing in direction of tilted turn-table rotation. (b) A capillary-sized droplet (~ 0.029 mL) in a 6.35 mm wide, 56 mm diameter channel. (c) A droplet of 25 g/L aqueous salt solution rolls along the superhydrophobic channel held at 170°C. Image taken at t=0 s. The droplet evaporates in time (d) t=56 s and (e) t=110 s. (f) Complete distillation leaves a single salt crystal in the channel, t=164 s.

tube provides a mechanism for local liquid acceleration which adds enough local inertia to the liquid that a jet is spontaneously ejected from the nozzle. This jet breaks up into droplets which are then employed downstream in dynamic Leidenfrost impact experiments. Figure 5 shows passive capillary ejection of 5 cS PDMS (Polydimethylsiloxane) fluid in a 60 mm long, 6 mm ID circular glass tube with a converging nozzle of 1.2 mm ID at the end of the tube.

C. Rolling Leidenfrost Droplets

An aluminum plate with 6.35 mm wide hemi-circular section milled circular track 56 mm in diameter is mounted to a turntable. The turntable is then tilted with respect to gravity and mounted to a table. The plate surface is coated with a superhydrophobic coating consisting of a PTFE spray (Dome MagicTM) over a soot layer deposited by candle flame, a method developed by Rasheed and Weislogel.⁴⁸ Figure 6 provides images of the apparatus with top-view images of the circular track with a capillary-sized droplet of 25 g/L aqueous NaCl mixture inside the track. A variable speed DC motor is used to drive the turn-table with mounted aluminum

plate. To the aluminum plate is mounted a 150-Watt strip heater controlled via Arduino control circuit comprised of thermocouples, ambient temperature thermocouple, humidity sensor, solid-state relays, and Arduino SD Shield for data acquisition.

The Arduino controller is programmed to establish the plate temperature. Once the setpoint temperature is reached, a droplet is dispensed in the channel while simultaneously turning on the DC turntable motor. A highspeed HD video camera records the events. The combined effects of plate rotation, plate tilt with respect to gravity, superhydrophobicity, and Leidenfrost temperatures cause the droplet to roll ever-downwards along the channel. The droplet continues to roll until completely evaporated. Figure 6c shows an image of a droplet at the beginning of one such experiment with plate temperature of 170° C. The 25 g/L aqueous NaCl droplet initial volume is ~ 0.029 mL. Figures 6d and e provide images of the droplet at t = 56 s and t = 110 s, respectively. Figure 6f provides an image of the salt crystal left behind following complete evaporation at t = 164 s. From these experiments we establish maximum Leidenfrost evaporation rates via droplet lifetime measurements. Such rates can be used to estimate envelope and performance metrics for low-g Leidenfrost distillation devices. The experiments also provide insight on fouling mechanisms for superhydrophobic surfaces due to complete distillation and deposition of salt solutions.

III. Mathematical Model

A. Dynamic Leidenfrost Droplet Impact in Microgravity: The Creeping Velocity Limit

We suspect that Leidenfrost behavior will be significantly impacted for low velocity impacts in a low-gravity environment. Thus, we pursue an order of magnitude assessment of the Leidenfrost vapor layer thickness for a free-flying, low-velocity droplet approaching a planar heated substrate well above the Leidenfrost point in a zero-gravity environment. A schematic of the problem is provided in Fig. 7. Neglecting drag in the gas phase, the approach of the droplet to the wall is modeled using a force balance where the acceleration of the droplet is set equal to the momentum of evaporation from the droplet in the direction of the wall; namely,

$$m\ddot{x} = \dot{m}_{evap} u_{vap},\tag{1}$$

where m is the droplet mass, \ddot{x} is the droplet acceleration toward the planar surface, \dot{m}_{evap} is the mass flowrate of vapor evaporating from the droplet, and u_{vap} is the vapor velocity leaving the droplet. From mass conservation, the vapor velocity may be expressed in terms of vapor mass flowrate, which in turn may be expressed in terms of heat transfer to the droplet q via energy balance $q = \dot{m}_{evap}(c_p\Delta T + h_{fg})$, where c_p is the droplet specific heat and ΔT is the difference between the droplet saturation temperature and initial droplet temperature, $\Delta T = T_d - T_o$. The zeroth order mode of heat transfer to the droplet is conduction from the heated planar substrate through the vapor layer of the droplet δ , which can be expressed as $\delta = x_o - x$. Scaling laws show that convection and radiation are negligible. Substitution for the vapor velocity and mass flowrate with conduction as the sole mode of heat transfer, the governing equation of motion becomes the simple nonlinear ODE

$$m\ddot{x} = \frac{\bar{k}}{(x_0 - x)^2},\tag{2}$$

where

$$\bar{k} \equiv \left[\frac{k_{\nu} (T_{s} - T_{d})}{c_{p} \Delta T + h_{fg}} \right]^{2} \frac{A}{\rho_{\nu}},\tag{3}$$

where k_v is the droplet vapor conductivity, T_s and T_d are the respective planar substrate and droplet saturation temperatures, A is the droplet frontal area, and ρ_v is the droplet vapor density. Scaling Eq. 2 with $x \sim x_f$ and $t \sim x_f/u_o$, and solving for x, a scale expression for the vapor layer thickness is found to be

$$\delta \sim x_0 - \frac{2B + 1 - \sqrt{4B + 1}}{(2B/x_0)},\tag{4}$$

where parameter $B = x_0 m u_0^2/\bar{k}$, which is a dimensionless ratio of droplet kinetic energy to energy of vaporization. From Eq. 4 the vapor layer thickness of a 5 mL droplet of water initially at 20°C travelling at 1 mm/s toward a substrate at 400°C from an initial distance of 100 mm yields $\delta \sim 5.7$ mm—an unearthly large thickness 3-orders of magnitude larger than terrestrial thicknesses. ^{13,30,51} The potentially and comparatively enormous vapor layer thicknesses predicted

by Eq. 4 for low velocity impacts suggest that low-g droplet flows along conduits, where normal velocities approach zero, a far more likely to remain 'un-impacted' and thus remain 'uncontaminated' when compared to our terrestrial demonstrations. The results suggest a significantly enhanced non-contact nature of the Leidenfrost phenomenon in microgravity.

B. Rolling Leidenfrost Droplet Lifetime

A simple mathematical model describing the heat transfer from a hot surface to a rolling droplet in Leidenfrost state on a superheated surface is developed. Figure 8 provides a schematic of a droplet with saturation temperature T_d rolling with linear velocity u on a superheated surface with temperature T_s and tilt angle α . The droplet has a radius r(t) that varies with time as it evaporates in the Leidenfrost state in an environment with ambient temperature T_∞ . We consider all modes of heat transfer to the rolling droplet, including conduction, forced and free convection, and radiation. A scale expression is derived for the Leidenfrost vapor layer thickness in gravity from a balance between vapor and hydrostatic pressures resulting in,

$$\delta \sim \left(\frac{\mu_v k_v \Delta T_1}{2\rho_l \rho_v g(c_P \Delta T_2 + h_{fg})}\right)^{1/3},\tag{5}$$

where μ_v is the droplet vapor viscosity, ρ_l is the liquid droplet density, ρ_v is the droplet vapor density, g is gravitational acceleration, $\Delta T_1 = T_s - T_d$ is the difference between plate temperature and droplet saturation temperature, and $\Delta T_2 = T_d - T_o$ is the difference between droplet saturation temperature and initial droplet temperature. Using Eq. 5, an expression for steady conduction heat transfer to the droplet from the heated substrate through the vapor layer can be expressed as

$$q_c = \pi r^2 (k_v \Delta T_1)^{2/3} (2\rho_l \rho_v g (c_p \Delta T_2 + h_{fg}) \mu_v^{-1})^{1/3}.$$
(6)

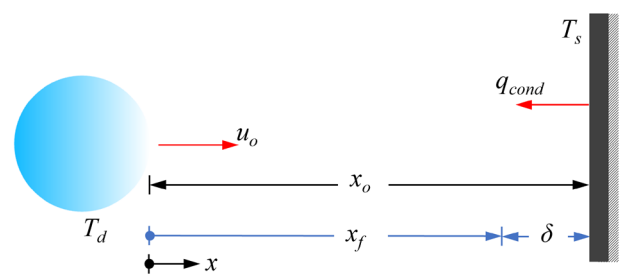


Figure 7: A free flying droplet in microgravity with temperature T_d approaching a planar superheated substrate. Conduction is the zeroth-order mode of heat transfer to the droplet. The droplet reaches a final distance x_f before rebounding, separated by a vapor layer δ .

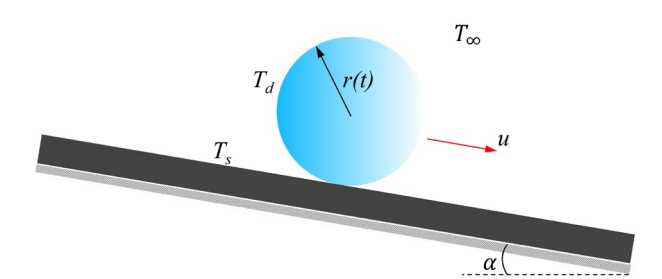


Figure 8: A droplet rolling with linear velocity \boldsymbol{u} on a heated tilted substrate well in excess of the Leidenfrost point.

In this case, order of magnitude comparisons suggests that conduction and forced convection are significantly more relevant than free convection and radiation. The convective heat transfer coefficient is estimated using the Whitaker correlation⁴⁷ for the average Nusselt Number for a sphere. From Newton's law of cooling, an expression for convective heat transfer to the droplet is expressed as

$$q_{fc} = 2\pi r k_a \Delta T_3 \left[2 + \left(0.4[Rr]^{1/2} + 0.06[Rr]^{2/3}\right) \Pr^{0.4} \left(\frac{\mu_{\infty}}{\mu_s}\right)^{1/4}\right],\tag{7}$$

where $R \equiv 2\rho_a u/\mu_a$, and k_a , μ_a , and ρ_a are the respective air thermal conductivity, dynamic viscosity, and density. Velocity u is that of the droplet, Pr the Prandtl number of air, μ_{∞} the air free stream dynamic viscosity, μ_s the air dynamic viscosity at plate surface temperature T_s and $\Delta T_3 = T_d - T_a$ is the difference between droplet saturation temperature T_a and air free stream temperature T_a . All properties for air are taken at the bulk temperature $T_b = (T_s + T_{\infty})/2$. The mass rate of change for an evaporating spherical droplet can be expressed as

$$\dot{m} = -4\pi \rho_l r^2 r_t,\tag{8}$$

where r_t is the time rate of change of the droplet radius. The evaporative mass flowrate can be expressed in terms of the total heat transfer to the droplet using the expression $q = \dot{m}(c_p \Delta T + h_{fg})$, substitution into which Eqs. 6-8 yield a first order non-linear ODE describing the droplet lifetime

$$r_{t} + \frac{k_{a}}{2\rho_{l}(c_{p}\Delta T_{2} + h_{fg})r} \Delta T_{3} \left[2 + r^{1/2} \left(0.4R^{1/2} + 0.06R^{2/3}r^{1/6} \right) \Pr^{0.4} \left(\frac{\mu_{\infty}}{\mu_{s}} \right)^{1/4} \right] + \frac{1}{4} \left(\frac{k_{v}\Delta T_{1}}{\rho_{l}\mu_{v}^{1/2}(c_{p}\Delta T_{2} + h_{fg})} \right)^{2/3} (2\rho_{v}g)^{1/3} = 0.$$

$$(9)$$

Eq. 9 is solved numerically with initial droplet radius condition $r(t=0)=R_o$, predicting the overall rolling droplet lifetime on a heated surface with constant velocity in the Leidenfrost state. The analytical result of Eq. 9 is compared to the experimentally measured Leidenfrost droplet lifetime results to assess the accuracy of the model. Solutions to Eq. 9 provide Leidenfrost droplet evaporation rates and lifetimes, both of which are useful for sizing a Leidenfrost droplet distiller.

IV. Results and Discussion

A. Microgravity

1. High Velocity Leidenfrost Impacts

Microgravity Leidenfrost droplet impact experiments are conducted with droplet impacts at various Weber numbers $We = \rho u^2 D/\sigma$, impact angles, surface temperature, surface wettability, and surface geometry. Figure 9 shows a series of images taken at 15 Hz for a 1.3 mL droplet of water impacting a superhydrophobic substrate held at 140°C in microgravity. A Logan Shooter is used to eject the water droplet free of oscillations toward the heated substrate with a normal velocity of 13.0 cm/s and a perpendicular impact Weber number of 3.1. The droplet impacts the substrate and elastically rebounds without undergoing nucleate boiling.

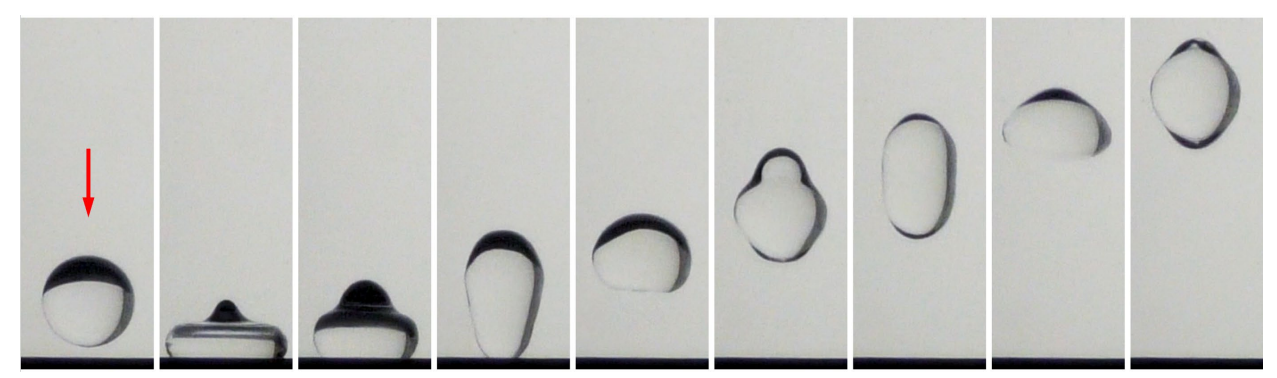


Figure 9: A sequence of images taken at 15 Hz of a 1.3 mL water droplet impacting a superhydrophobic substrate held at 140°C in microgravity. The droplet is ejected out of a Logan Shooter, free of oscillations, normal relative to the surface at a velocity of 13.0 cm/s with a normal impact Weber number equal to 3.1.

A series of low-g dynamic Leidenfrost impact experiments are shown in Fig. 10 where oscillation-free water droplets are ejected from a Logan Shooter toward the heated substrate. Figures 10a and 10b show a series of images taken at 6 Hz from impacts on polished aluminum at 206°C and a superhydrophobic surface at 142°C, respectively. Incoming impact angles are 45° and perpendicular Weber numbers are 1.9 for both experiments. Elastic rebounds are observed in both experiments with outgoing impact angles of 42° for the impact on the aluminum plate and 45° for the impact on the superhydrophobic plate. It is clear from such demonstrations that for fixed impact Weber number, superhydrophobic surfaces drastically reduce the dynamic Leidenfrost point in microgravity.

Figure 10c shows images taken at 6 Hz for a droplet impacting a superhydrophobic array of circular pillars, held at 140°C with pillar diameters of 0.9 mm and pillar spacings of 0.8 mm. The incoming and outgoing impact angles are observed to be 45° with perpendicular impact Weber number of 2.1. An elastic rebound is observed free of nucleate boiling. The droplet impact in Fig. 10c results in a droplet with higher mode oscillations on the surface of the droplet after impact compared to the aluminum surface rebound (10a) and superhydrophobic plate impact (10b) due to droplet deformation into the pillar gaps during impact. Figure 10d shows a series of images taken at 12 Hz of a 1.5 mL droplet of water painted with UV dye impacting a stainless-steel cylinder with a Weber number of 2.1. The cylinder is 9.5

mm in diameter at 465°C. The droplet impacts and rebounds from the cylinder elastically apparently initiating a degree of rigid body rotation.

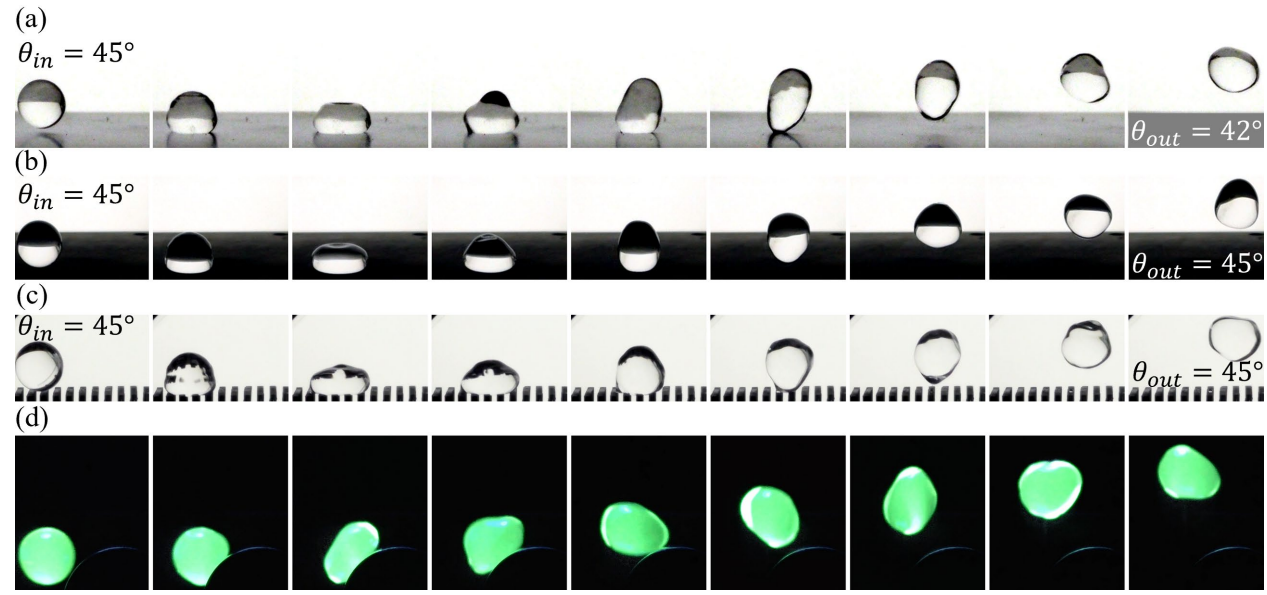


Figure 10: Sequence of images of oscillation-free water droplet impacts for droplets ejected using a Logan Shooter. (a) Sequence of 6 Hz images of a 12.6 cm/s 1.1 mL droplet impact at 45° on a polished aluminum substrate at 206°C, rebound angle is 42° likely due to viscous drag on impact. (b) 12.3 cm/s 1.2 mL droplet impacting a superhydrophobic surface at 142°C, rebound angle is 45°. (c) 13.2 cm/s 1.0 mL droplet impacting a superhydrophobic array of 0.9 mm diameter circular pillars and 0.8 mm spacing at 140°C, rebound angle is 45°. (d) 12 Hz images of 10.4 cm/s 1.5 mL droplet painted with UV fluorescent dye impacting a 9.5 mm diameter stainless-steel cylinder at 465°C.

Low-gravity Leidenfrost droplet impact experiments between two parallel plates were also conducted. Shown in Fig. 11 are image overlays from three experiments taken at 30 Hz of 1 mL water droplets ejected with a Logan Shooter into two parallel plates separated by a distance of 13.5 mm with overall length of 127 mm. Figure 11a is a water droplet bouncing between two superhydrophobic plates at room temperature with initial velocity of 31.9 cm/s and final velocity of 23.2 cm/s. The sum of incident and reflection angles $\theta_i + \theta_R$ increases from 93° to 100° over the course of five bounces. Figure 11b shows the same experiment, but with heated superhydrophobic plates, with the top and bottom plates at 168°C and 183°C, respectively. Droplet velocity decreases from 25.1 cm/s to 21.1 cm/s and the sum of incident and reflection angles decrease from 103° to 97° over the course of five bounces. Figure 11c shows the same experiment as in Fig. 11a and 11b, but with superheated polished aluminum surfaces with top and bottom plates held at 305°C and 366°C, respectively. Droplet velocity decreases from 26.7 cm/s to 15.6 cm/s and the sum of incident and reflection angles decrease from 110° to 84° over the course of five bounces. The heated plate experiments, unlike the non-heated plate experiment, observed decreases in the sum of incident and reflection angles. The experiment in Fig. 11c displays a greater decrease compared to the heated superhydrophobic plate experiment in Fig. 11b likely due to increased Leidenfrost vapor recoil forces, which propel the droplets in a predominately perpendicular direction to the substrates. A larger decrease in the sum of incident and reflection angles indicates a larger vapor recoil force, which is observed in the superheated plates experiment. In the absence of gravity, the Leidenfrost vapor recoil force plays a more controlling role in the droplet behavior which may be exploited in practical systems design for spacecraft.

2. Leidenfrost Fluid Transport in Conduits

Low-g Leidenfrost experiments investigating fluid transport in circular conduits with bends were performed. Figure 12a shows 17 Hz images of an experiment where blue-dyed ethanol droplets are ejected using the passive capillary ejection method (ref. Fig. 5). The 60 mm long 9 mm ID glass tube ejector with converging nozzle of 1.5 mm ID exit was used. The glass receiving tube has a 45° bend at the outlet and is heated to $> 360^{\circ}$ C. The glass tube has an 8.5 mm ID and is 63 mm in length. Ejected droplet diameters are 1.9 mm, with the largest velocity droplet ejected

at 38.4 cm/s resulting in We = 10. Elastic Leidenfrost impacts are observed and the droplets successfully traverse the conduit and exit without wetting/touching any surfaces. Figure 12b shows 15 Hz images of a similar test where ethanol is ejected from the same nozzle as in Fig. 12a, but into a glass tube with 180° bend. This tube has a 4 mm ID and 64 mm length and is heated to > 360°C. Droplets ejected into the tube are 1.8 mm in diameter with the largest velocity of 41.6 cm/s, resulting in We = 11. All droplets rebound elastically in the Leidenfrost state, traversing the bend and exiting the tube without wetting any surfaces. Figure 12c shows 17 Hz images of a pressure driven jet of blue-dyed ethanol from a 20-gauge needle, which breaks up via Plateau-Rayleigh instability into a stream of droplets. This droplet stream is ejected into the same glass tube as in Fig. 12b, heated to > 360°C. The ejected droplets have maximum

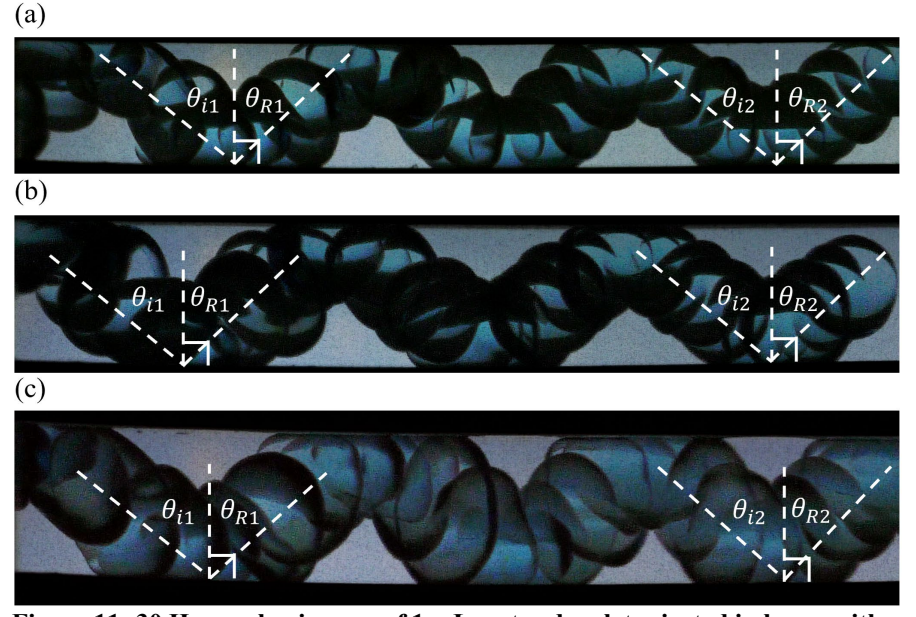


Figure 11: 30 Hz overlay images of 1 mL water droplets ejected in low-g with a Logan Shooter bouncing 5 times between parallel plates. The 127 mm long plates are separated by a distance of 13.5 mm. (a) Two superhydrophobic plates at room temperature: velocity decreases from 31.9 cm/s to 23.2 cm/s and $\theta_i + \theta_R$ increase from 93° to 100°. (b) Two heated superhydrophobic plates with the top and bottom plates at 168°C and 183°C, respectively. Droplet velocity decreases from 25.1 cm/s to 21.1 cm/s and $\theta_i + \theta_R$ decrease from 103° to 97°. (c) Two polished aluminum plates with top and bottom plates at 305°C and 366°C, respectively. Droplet velocity decreases from 26.7 cm/s to 15.6 cm/s and the sum of $\theta_i + \theta_R$ decrease from 110° to 84°.

diameters of 2.6 mm and average velocity of 22.0 cm/s, resulting in We = 4.5. The entire stream of droplets traverses the bend, making it through the conduit without contact, wetting or nucleate boiling.

Ethanol Leidenfrost jet experiments in microgravity are conducted in coiled glass tubing. Figure 13 shows 60 Hz overlay images for three experiments where jets of ethanol are ejected into the superheated 6 mm ID glass coiled on an 85 mm OD at > 360°C. The pressure-driven ethanol jets are again ejected through a 20-gauge syringe. Figure 13a shows an overlay of a test where the jet is ejected into the superheated glass coil with an open inlet. The jet breaks up into a stream of droplets that traverse the coil bends in the non-contact Leidenfrost mode. Droplets exit out of the outlet of the coil as identified by the red arrow. However, a buildup of droplets is observed near the inlet of the coil caused by vapors produced

expanding both up and down stream, effectively halting the flow. When the inlet is sealed, as is the case in Fig. 13b, the ethanol jet evenly distributes throughout the coil and no buildup of fluid in the coil at the inlet is observed, the vapors produced propelling the droplets downstream and out of the coil. In Fig. 13c the same test is conducted, but with the addition of a 5.5 Lpm airflow through the coil and an open inlet. An even distribution of droplets is observed as in the experiment shown in Fig. 13b where no droplet buildup occurs. Such demonstrations provide ready examples of how essentially passive non-contact droplet delivery and Leidenfrost transport methods can be achieved in conduits. Based on such tests, a prototypical distillation system may require as little as ~ 15 m length of tubing for complete distillation.

3. Low-Velocity Leidenfrost Impact

Low velocity Leidenfrost droplet impact experiments in microgravity were conducted. Weber numbers on the order of 10⁻⁴ or less are desired to produce millimetric vapor layer thicknesses predicted in Eq. (4) for low velocity Leidenfrost impacts. Ethanol and liquid nitrogen are used in these demonstration experiments for their relatively low specific heat and latent heat of vaporization. Liquid nitrogen is of particular interest for such experiments due to its low saturation temperature –195.8°C making room temperature surfaces Leidenfrost temperature surfaces.

Passive capillary ejection of ethanol droplets into a converging nozzle toward heated surfaces at low impact angles were performed in microgravity. Figure 14 shows 120 Hz image overlays of a 1.9 mm ejected droplet of ethanol impacting a superheated plate at 400°C. The incoming velocity and angle of the droplet are 11.7 cm/s and 2.3°, respectively, resulting in perpendicular impact speed and perpendicular Weber number of 4.7 mm/s and 0.0015, respectively. The outgoing speed and angle are 11.4 cm/s and 7.6°, respectively, with perpendicular exit velocity of 15.1 mm/s. The three-fold increase in perpendicular velocity from pre- to post-impact suggests the magnitude of acceleration induced by droplet vaporization, which is readily detected. This force may be used to solve inversely for the evaporation rates for a more quantitative assessment of the assumptions leading to Eq. (4). Further analytical comparisons will be reported at a later date.



Figure 12: Microgravity Leidenfrost droplet experiments in glass tubes. (a) Passive capillary ejection of blue-dyed ethanol droplets: 17 Hz images of 38.4 cm/s, 1.9 mm droplets into an 8.5 mm ID 63 mm long glass tube bent 45° at one end and held at > 360°C. (b) 15 Hz images of 41.6 cm/s, 1.8 mm ethanol ejected into 4.0 mm ID, 63 mm long tube with 180° bend. (c) 17 Hz images of a pressure driven ethanol jet ejected from a 20-gauge needle into the glass tube of (b), producing 2.6 mm droplets at average velocity 22 cm/s.

To further investigate vapor recoil forces impacting Leidenfrost phenomena in low-g environments, a series of drop tower tests were conducted to establish perpendicular Weber numbers $\sim 10^{-4}$ or less, where droplets of liquid nitrogen are ejected parallel to a superheated substrate. Liquid nitrogen droplets are ejected using an aluminum Logan Shooter, where the non-wetting function is performed by the Leidenfrost vapor layer for liquid nitrogen instead of superhydrophobic surfaces for water, as was demonstrated in Fig. 4. Figure 15 shows 120 Hz overlay images of a liquid nitrogen droplet ejected nearly parallel to a heated surface at 450°C. The 1.7 mm droplet is ejected at speed of 60.6 cm/s at an approximately 0.2° impact angle. The ejection location is 2.7 mm above the planar heated substrate. The droplet traverses over the heated surface for a 0.61 s duration. While traversing the surface, the drop is redirected away from the surface to a distance of 3.9 mm after 370 mm of travel. The total deflection caused by vapor recoil forces is $\delta = 1.2$ mm. From the scale expression of Eq. 4, we estimate a vapor layer thickness of 1.6 mm for this outcome, which is in fair agreement with the experimental observations.

B. Terrestrial Leidenfrost Droplet Evaporation

To estimate droplet residence time in a 'Leidenfrost distiller,' droplet lifetime experiments are conducted using the rotating, heated superhydrophobic Leidenfrost channel apparatus described in Section 2C. The capillary-sized

droplets of distilled water with initial volume ~ 0.029 mL are deployed in the superhydrophobic channel held at 170°C. Figure 16 provides a plot of droplet lifetimes as a function of linear droplet velocity for various plate tilt angles. Also plotted are the droplet lifetime results from numerical solutions to Eq. 9.

The experimental results show a general decrease in droplet lifetime for all tilt angles as droplet velocity is increased due to increases in convective heat transfer. This trend is captured in the analytical results as well. For the same droplet velocity, droplet lifetime decreases as tilt angle is increased. This is due to increased droplet contact area with the heated plate due to the semi-circular cross-sectional geometry of the heated channel. Conduction is the dominant mode of heat transfer and as a result, increased contact area plays a large role in determining the droplet lifetime. This is not captured in the analysis since the solution for the droplet lifetime assumed a droplet rolling on a flat surface. Overall, the analytical model predicts droplet lifetimes reasonably well for tilt angles of 15° or lower, with maximum deviation of \pm 30% for all experimental results conducted.



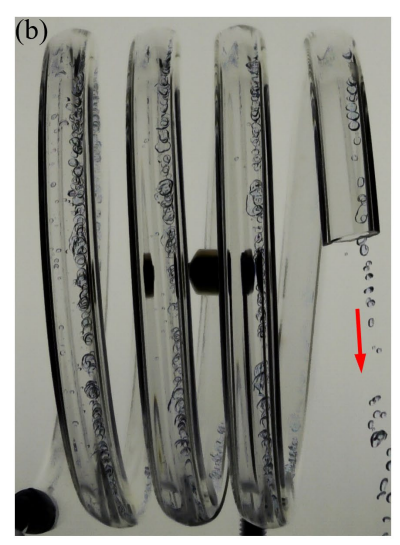




Figure 13: 60 Hz overlay images for three drop tower tests where jets of dyed ethanol are ejected into a 6 mm ID glass coil with OD of 85 mm at > 360°C: (a) Jet of ethanol ejected into a superheated glass coil with an open inlet and no airflow, (b) jet ejected with a plugged inlet and no airflow, and (c) jet ejected with open inlet and 5.5 Lpm airflow.



Figure 14: An image overlay, taken at 120 Hz, of a 1.9 mm droplet of ethanol with incoming velocity, u_i , of 11.7 cm/s and incoming, θ_i , and outgoing angles, θ_e , of 2.3° and 7.6°, respectively. Normal impact Weber number was found to be 1.5*10⁻³. Incoming and outgoing normal velocities were found to be 4.7 mm/s and 15.1 mm/s, respectively.



Figure 15: 120 Hz image overlay for a 1.7 mm liquid nitrogen droplet ejected at 60.6 cm/s from a Logan Shooter, nearly parallel to a planar surface at 450° C. The droplet has an impact angle of $\sim 0.2^{\circ}$, and is ejected 2.7 mm away from the wall, before being propelled upward due to vapor recoil forces and ending up 3.9 mm from the wall. Measured vapor layer thickness is 1.2 mm.

To demonstrate temperature, pressure, and concentration effects, droplet distillation experiments are conducted using the same apparatus but employing flat beer, urine, and 25 g/L aqueous solutions of NaCl, KCl, and sugar. Controlled solute-solvent separation is also observed for all fluids used. An example of solute-solvent separation is shown in Fig. 6 for separation of water and NaCl. Deposition of solutes on the superhydrophobic surface was observed. The surface was fouled from the dissolved solutes in solutions precipitating out of solution near the end of all tests performed. The ability to clean the heated superhydrophobic surface from deposited solutes from the various solutions is easily demonstrated, exploiting the 'self-cleaning' nature of such surfaces. For example, dispensing a droplet of water into the rotating channel readily re-dissolves the solutes, cleaning the surface, and recovering the superhydrophobic characteristics of the surface to pre-experiment conditions. These observations again demonstrate additional favorable attributes for a Leidenfrost distillation system promoting non-contact distillation.

V. Summary

Terrestrial and microgravity investigations of the Leidenfrost phenomenon relevant to potential application aboard spacecraft life support systems have been presented. Analytical models are presented that predict Leidenfrost vapor layer thicknesses in microgravity for low velocity droplet impacts. A model for dynamic Leidenfrost droplets rolling on heated surfaces is also presented accounting for conduction and forced convection heat transfer to the droplets.

Novel microgravity Leidenfrost impact experiments are presented showcasing a variety of high-velocity dynamic Leidenfrost impacts on planar surfaces, surfaces with macro-roughness, and surfaces with cylindrical cross-sectional geometry in short duration drop tower tests. Also demonstrated are Leidenfrost droplet transport experiments through tortuous conduits in microgravity where droplets and streams of droplets are ejected through superheated tubes of varying lengths, diameters, and pathway geometry. Droplet transport between plates is presented where it is found that droplets bouncing between two parallel superheated plates experience decreases in incident and reflected angles due to Leidenfrost vapor recoil forces acting perpendicular to the impacted surfaces. This vapor recoil force is observed in low-velocity impacts where ethanol droplets are shown to propel away from superheated surfaces at increased normal velocity. In perhaps a first observation, the production of a large 'millimetric' vapor layer thickness of a liquid nitrogen droplet ejected nearly parallel to a superheated surface was achieved. The observed deflection of the droplet was measured to be 1.2 mm, which is in good agreement with the analytical prediction from Eq. 4 of 1.6

> mm for the vapor layer thickness. Terrestrial vapor layers are typically 'micro-metric.'

> To estimate possible performance of such in processes the sustained environment of orbiting spacecraft, terrestrial Leidenfrost droplet lifetime experiments are presented for a stationary drop on a rotating Leidenfrost stage. The results show decreased droplet lifetime with increased droplet velocity, as well as a general decrease in droplet lifetime with increased tilt angles. Results from the mathematical model developed compare well with experimental results. The analyses capture general droplet lifetime trends as well as overall droplet lifetimes to within \pm 30%. The tests performed herein are supported by analyses that show how Leidenfrost phenomena is significantly enhanced in low-g environments.

> With this knowledge, the utility of Leidenfrost phenomenon in microgravity is revealed as an attractive means of establishing essentially non-contact methods of fluids transport aboard spacecraft. For the present example, both experimental and

2.5° Tilt 0 7.5 10 200 15° 40° Droplet Lifetime (s) 180 Eq. (9) 160 0 # 8 \Diamond 0 120 100 10 15 20 25 30 Droplet Velocity (cm/s)

220

Figure 16: Droplet lifetime vs. droplet velocity for ~ 0.029 mL droplets of distilled water in a superhydrophobic semi-circular channel at 170°C at varying tilt angles, with comparisons to analytical model of Eq. 9.

theoretical results for Leidenfrost droplet lifetime and evaporation rates can serve as preliminary design tools for a Leidenfrost distillation system. We demonstrate non-contact microgravity Leidenfrost droplet impact phenomena on a variety of surface geometries for a variety of impact conditions. Leidenfrost droplet impacts in circular conduits are particularly applicable to practical microgravity distiller design. We also show how the addition of superhydrophobicity drastically reduces Leidenfrost temperatures for water from ~ 206°C to as low as ~ 140°C in microgravity. Such superhydrophobic substrates are observed to reduce fouling substantially, with fouled superhydrophobic surfaces capable of recovering their non-wetting characteristics after a simple rinse with clean water. These demonstrations encourage further exploitation of Leidenfrost phenomena towards fluids processing

applications aboard spacecraft, such as water recovery via non-contact distillation from contaminated water sources for life support.

Acknowledgments

This work was supported in part by NASA Space Technology Research Fellowship titled Leidenfrost Driven Waste-Water Separator, September 15, 2017: CoTR – Jennifer Pruitt.⁵⁰

References

¹Leidenfrost, J. G. (1756). *De aquae communis nonnullis qualitatibus tractatus*. Ovenius.

²Quéré, D. (2013). Leidenfrost dynamics. *Annual Review of Fluid Mechanics*, 45, 197-215.

³Stamey, T. A., & Mihara, G. (1980). Observations on the growth of urethral and vaginal bacteria in sterile urine. *The Journal of Urology*, 124(4), 461-463.

⁴Itaru, M., & Kunihide, M. (1978). Heat transfer characteristics of evaporation of a liquid droplet on heatedsurfaces. *International Journal of Heat and Mass Transfer*, 21(5), 605-613.

⁵Avedisian, C. T., & Koplik, J. (1987). Leidenfrost boiling of methanol droplets on hot porous/ceramicsurfaces. *International Journal of Heat and Mass Transfer*, 30(2), 379-393.

⁶Bernardin, J. D., Stebbins, C. J., & Mudawar, I. (1997). Mapping of impact and heat transfer regimes

of water drops impinging on a polished surface. International Journal of Heat and Mass Transfer, 40(2), 247-267.

⁷Rein, M. (2002). Interactions between drops and hot surfaces. In *Drop-Surface Interactions* (pp. 185-217). Springer, Vienna.

⁸Abramzon, B., & Sazhin, S. (2005). Droplet vaporization model in the presence of thermal radiation. *International Journal of Heat and Mass Transfer*, 48(9), 1868-1873.

⁹Wu, G., & Sirignano, W. A. (2011). Transient convective burning of interactive fuel droplets in double layer arrays. *Combustion and Flame*, *158*(12), 2395-2407.

¹⁰Sazhin, S. S., Krutitskii, P. A., Gusev, I. G., & Heikal, M. R. (2010). Transient heating of an evaporating droplet. *International Journal of Heat and Mass Transfer*, *53*(13-14), 2826-2836.

¹¹Gradeck, M., Ouattara, A., Maillet, D., Gardin, P., & Lebouché, M. (2011). Heat transfer associated to a hot surface quenched by a jet of oil-in-water emulsion. *Experimental Thermal and Fluid Science*, *35*(5), 841-847.

¹²Tarozzi, L., Muscio, A., & Tartarini, P. (2007). Experimental tests of dropwise cooling on infrared transparent media. *Experimental Thermal and Fluid Science*, *31*(8), 857-865.

¹³Biance, A. L., Clanet, C., & Quéré, D. (2003). Leidenfrost drops. *Physics of Fluids*, 15(6), 1632-1637.

¹⁴Quere, David (2013). "Leidenfrost Dynamics." Annu. Rev. Fluid Mech. 45:197–215., doi: 10.1146/annurev-fluid-011212-140709

¹⁵Tran, T., Staat, H. J., Prosperetti, A., Sun, C., & Lohse, D. (2012). Drop impact on superheated surfaces. *Physical Review Letters*, 108(3), 036101.

¹⁶Yao, S. C., & Cai, K. Y. (1988). The dynamics and Leidenfrost temperature of drops impacting on a hot surface at small angles. *Experimental Thermal and Fluid Science*, *1*(4), 363-371.

¹⁷Tran, T., Staat, H. J., Susarrey-Arce, A., Foertsch, T. C., van Houselt, A., Gardeniers, H. J., ... & Sun, C. (2013). Droplet impact on superheated micro-structured surfaces. *Soft Matter*, *9*(12), 3272-3282.

¹⁸van Limbeek, M. A., Shirota, M., Sleutel, P., Sun, C., Prosperetti, A., & Lohse, D. (2016). Vapour cooling of poorly conducting hot substrates increases the dynamic Leidenfrost temperature. *International Journal of Heat and Mass Transfer*, 97, 101-109.

¹⁹Gradeck, M., Seiler, N., Ruyer, P., & Maillet, D. (2013). Heat transfer for Leidenfrost drops bouncing onto a hot surface. *Experimental Thermal and Fluid Science*, *47*, 14-25.

²⁰Park, J., & Kim, H. (2016). An experimental investigation on dynamics and heat transfer associated with a single droplet impacting on a hot surface above the Leidenfrost point temperature. *Kerntechnik*, 81(3), 233-243.

²¹Dunand, P., Castanet, G., Gradeck, M., Maillet, D., & Lemoine, F. (2013). Energy balance of droplets impinging onto a wall heated above the Leidenfrost temperature. *International Journal of Heat and Fluid Flow*, 44, 170-180.

²²Dunand, P., Castanet, G., Gradeck, M., Lemoine, F., & Maillet, D. (2013). Heat transfer of droplets impinging onto a wall above the Leidenfrost temperature. *Comptes Rendus Mécanique*, *341*(12), 75-87.

²³Xie, H., & Zhou, Z. (2007). A model for droplet evaporation near Leidenfrost point. *International Journal of Heat and Mass Transfer*, 50(25-26), 5328-5333.

²⁴Orzechowski, T., & Wciślik, S. (2014). Analysis of D2-law in case of Leidenfrost drop evaporation. *Experimental Thermal and Fluid Science*, *59*, 230-237.

- ²⁵Maquet, L., Brandenbourger, M., Sobac, B., Biance, A. L., Colinet, P., & Dorbolo, S. (2015). Leidenfrost drops: Effect of gravity. *EPL (Europhysics Letters)*, 110(2), 24001.
- ²⁶Veldhoven, A., & Capelleveen, B. F. (2014). *Ambient air pressure influence on the dynamic Leidenfrost temperature of impacting droplets* (Bachelor's thesis, University of Twente).
- ²⁷Chen, H., Cheng, W. L., Peng, Y. H., & Jiang, L. J. (2018). Dynamic Leidenfrost temperature increase of impacting droplets containing high-alcohol surfactant. *International J. of Heat and Mass Transfer*, 118, 1160-1168.
- ²⁸Takata, Y., Hidaka, S., Cao, J. M., Nakamura, T., Yamamoto, H., Masuda, M., & Ito, T. (2005). Effect of surface wettability on boiling and evaporation. *Energy*, *30*(2-4), 209-220.
- ²⁹Kim, S. H., Kang, J. Y., Ahm, H. S., Jo, H. J., & Kim, M. H. (2013). Study of Leidenfrost mechanism in droplet impacting on hydrophilic and hydrophobic surfaces. *International Journal of Air-Conditioning and Refrigeration*, 21(04), 1350028.
- ³⁰Kim, H., Truong, B., Buongiorno, J., & Hu, L. W. (2011). On the effect of surface roughness height, wettability, and nanoporosity on Leidenfrost phenomena. *Applied Physics Letters*, *98*(8), 083121.
- ³¹Kim, H., Truong, B., Buongiorno, J., & Hu, L. W. (2012). Effects of micro/nano-scale surface characteristics on the Leidenfrost point temperature of water. *Journal of Thermal Science and Technology*, 7(3), 453-462.
- ³²Lee, G. C., Kang, J. Y., Park, H. S., Moriyama, K., Kim, S. H., & Kim, M. H. (2017). Induced liquid-solid contact via micro/nano multiscale texture on a surface and its effect on the Leidenfrost temperature. *Experimental Thermal and Fluid Science*, *84*, 156-164.
 - ³³Kruse, C., Anderson, T., Alexander, D., Gogos, G., & Ndao, S. (2013, July). Controlling the Leidenfrost
- ³⁴Kruse, C., Anderson, T., Wilson, C., Zuhlke, C., Alexander, D., Gogos, G., & Ndao, S. (2013). Extraordinary shifts of the Leidenfrost temperature from multiscale micro/nanostructured surfaces. *Langmuir*, *29*(31), 9798-9806.
 - ³⁵Duursma, G. R., Kennedy, R. A., & Sefiane, K. (2014). The Leidenfrost phenomenon on structured surfaces.
- ³⁶Nair, H., Staat, H. J., Tran, T., van Houselt, A., Prosperetti, A., Lohse, D., & Sun, C. (2014). The Leidenfrost temperature increase for impacting droplets on carbon-nanofiber surfaces. *Soft matter*, *10*(13), 2102-2109.
- ³⁷Kwon, H. M., Bird, J. C., & Varanasi, K. K. (2013). Increasing Leidenfrost point using micro-nano hierarchical surface structures. *Applied Physics Letters*, *103*(20), 201601.
- ³⁸Arnaldo del Cerro, D., Marin, A. G., Römer, G. R., Pathiraj, B., Lohse, D., & Huis In't Veld, A. J. (2012). Leidenfrost point reduction on micropatterned metallic surfaces. *Langmuir*, 28(42), 15106-15110.
- ³⁹Vakarelski, I. U., Patankar, N. A., Marston, J. O., Chan, D. Y., & Thoroddsen, S. T. (2012). Stabilization of Leidenfrost vapour layer by textured superhydrophobic surfaces. *Nature*, 489(7415), 274.
- ⁴⁰Attari, B., Weislogel, M., Wollman, A., Chen, Y., & Snyder, T. (2016). Puddle jumping: Spontaneous ejection of large liquid droplets from hydrophobic surfaces during drop tower tests. *Physics of Fluids*, *28*(10), 102104.
- ⁴¹Wollman, A., Weislogel, M., Wiles, B., Pettit, D., & Snyder, T. (2016). More investigations in capillary fluidics using a drop tower. *Experiments in Fluids*, *57*(4), 57.
 - ⁴²Dryden Drop Tower Homepage: https://www.pdx.edu/dryden-drop-tower/
- ⁴³Wollman, A., Weislogel, M. (2013). New investigations in capillary fluidics using a drop tower. *Experiments in Fluids*, *54*(4), 1499.
- ⁴⁴Wollman A (2012) Capillarity-driven droplet ejection. Master's thesis, Portland State University. PermanentLink: http://archives.pdx.edu/ds/psu/8243
- ⁴⁵Torres L., M. Weislogel, S. Arnold, Capillary migration of large confined super-hydrophobic drops in wedges, 69th Ann. Meeting of the APS Division of Fluid Dynamics, Vol. 61, No. 20, D36.00006, Portland, Nov. 20–22, 2016.
- ⁴⁶Torres, L., Weislogel, M., Avhad, A., Tan, H., Large droplet generation by capillary migration in superhydrophobic wedges, 33rd Annual Meeting of the American Society for Gravitational and Space Research, ID306, Seattle, Oct. 25-28, 2017.
- ⁴⁷Whitaker, S. (1972). Forced convection heat transfer correlations for flow in pipes, past flat plates, single cylinders, single spheres, and for flow in packed beds and tube bundles. *AIChE Journal*, *18*(2), 361-371.
- ⁴⁸Rasheed, M. R., Weislogel, M. (2019, July). The Unrealized Potential of Superhydrophobic Substrates in Advanced Life Support Systems (In press).
- ⁴⁹Rasheed, R., Weislogel, M., Large Length Scale Leidenfrost Phenomena: Recent Results from Drop Tower Experimentation, 34th Annual Meeting of the American Society for Gravitational and Space Research, ID-237, Bethesda, Oct. 31-Nov. 3, 2018.
- ⁵⁰Original NSTRF Award Announcement, "Leidenfrost Driven Waste Water Separator": https://www.nasa.gov/directorates/spacetech/strg/nstrf 2017/Leidenfrost Driven Waste-Water Separator/
 - ⁵¹van Limbeek, M. A. J. (2017). The dynamics of Leidenfrost drops.